# Brain Tumor Segmention based on Dilated Convolution Refine Networks


Di Liu
School of Software
Yunnan University
Kunming, China
jorkzhang@163.com

Hao Zhang
School of Software
Yunnan University
Kunming, China
withoutrule14@gmail.com

Mingming Zhao
School of Software
Yunnan University
Kunming, China
mingzhaom@sina.com

Xiaojuan Yu
School of Software
Yunnan University
Kunming, China
juanxyu@126.com

Shaowen Yao*
School of Software
Yunnan University
Kunming, China
yaosw@ynu.edu.cn

Wei Zhou*
School of Software
Yunnan University
Kunming, China
zwei@ynu.edu.cn



***Abstract*— A brain tumor is a growth of abnormal cells in the tissues of the brain, which is difficult for treatment and severely affects patients' cognitive ability. Recent year magnetic resonance imaging (MRI) has been widely used imaging technique to assess brain tumors. However manual segmentation and artificial extracting features block MRI's practice when facing with the huge amount of data produced by MRI. An efficient and automatic image segmentation of brain tumor is still needed. In this paper, a novel automatic segmentation framework of brain tumors, which have 5 parts and resnet-50 use as a backbone, is proposed based on convolutional neural network. A dilated convolution refine (DCR) structure is introduced to extract the local features and global features. After investigating different parameters of our framework, it is proved that DCR is an efficient and robust method in Brain Tumor Segmentation. The experiments are evaluated by Multimodal Brain Tumor Image Segmentation (BRATS 2015) dataset. The results show that our framework in complete tumor segmentation achieved excellent results with a DEC score of 0.87 and a PPV score of 0.92.**
*(GitHub:https://github.com/wei-lab/DCR)*



***Keywords-brain tumor segmentation, convolutional neural networks, DCR, deep learning***


## I. INTRODUCTION

A brain tumor is a growth of abnormal cells in the tissues of the brain, which is difficult for treatment and severely affect patients' cognitive ability. Recent years with the gradual evolution of medical equipment, for malignant brain tumors some significant progress have been made in imaging, radiotherapy, chemotherapy and surgery， etc. However certain cases of malignant brain tumors are still considered untreatable with a 2.5-year cumulative relative survival rate of 8% and 2% at 10 years [1]. Previous studies have demonstrated that multimodal magnetic resonance imaging (MRI) features can guide the diagnosis, improve prediction rate and help for treatment planning [2, 3].

Specifically, a healthy brain usually consists of three types of tissue: white matter, gray matter, and cerebrospinal fluid. Brain tumors are easily integrated into these healthy tissues, which is fuzzy and hard to distinguish from healthy tissues. Currently, a series of MRI images have been generated by a magnetic resonance to complete the diagnosis of brain tumor. Figure 1 is a MRI example of a tumor patient. it has four different modalities, namely T1, T1C, T2 and Flair which are co-registered. The last one (i.e. Ground Truth image) is generated by combining the different patterns of the location and type of tumor in the previous 4 modalities. Note here different colors represent different tumor types and we totally have four types in this Ground Truth picture.

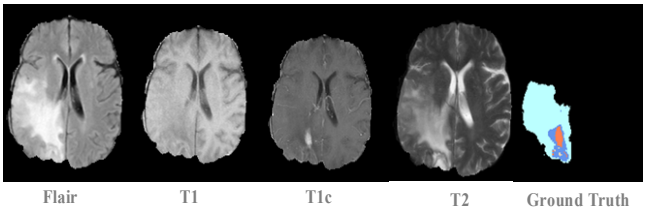


Fig. 1. An MRI example of a tumor patient

Magnetic resonance imaging (MRI) is a widely used imaging technique to assess brain tumors, which has great value in clinical medicine for accurately predicting the location and types of brain tumors. Image segmentation is a critical step for the MRI images to be used in brain tumor studies with three reasons: (1) Segmented brain tumors can eliminate confounding structures from other brain tissues. Therefore, this method can provide more accurate classification of brain tumors and effectively assist in subsequent diagnosis and treatment. (2) Accurately designing the crucial steps in the treatment of tumors during radiotherapy or surgery is not only the need to outline the extent of tumor expansion, but also the surrounding healthy tissue needs to be carefully excluded to avoid sensory functional site injury treatment; (3) The segmentation of longitudinal MRI scan can effectively monitor the recurrence, growth or contraction of brain tumors.

However most of the methods of brain tumors require the manual segmentation, which are time-consuming and laborious works when facing the huge amount of data produced by MRI. Besides, many previous works adopt artificial extracting features, and then using classical machine learning ways to train effective pixel-level classifiers by these artificially extracted features. But traditional machine learning methods for this pixel level based classification still have great deficiencies and reliance


978-1-5386-5886-4/18/$31.00 ©2018 IEEE
SERA 2018, June 13-15, 2018, Kunming, China

on prior knowledge. Therefore, some deep neural networks based methods have been proposed and achieved progress in recent years. Now more accurate features can be extracted by CNN, and the model discriminative ability is greatly improved. However, using CNN to implement an accurate and effective brain segmentation algorithm, we mainly consider two challenges. (1) A series of pooling operations are used by CNN for getting abstract features. However, this transformation seriously affects the brain tumor segmentation that requires accurate information. (2) Theoretically the size of Resnets' receptive field is larger than the input image, but Zhou *et al.* [4] found that the actual field of receptivity of CNN is much smaller than the theoretical receptive field, especially in high-level networks.

To address the above challenges, we develop dilated convolution refine based convolutional neural network (CNN) for brain tumor segmentation. The DCR-based CNN approach allows us to integrate the local features and global features well. Our DCR-based CNN approach is novel in three aspects: First, we introduce the encoder-decoder architecture and the Resnet work as a backbone in encoder phase. we obtained multi-scale features from different levels of Resnet, which makes up for the output of the encoder-decoder structure that originally can only provide a single high-level rough feature as a basis for the determination of defects. Second, A DCR structure is innovatively introduced into this network, which can be effectively expand the receptive field of the convolution kernel. After investigating different parameters of our framework, it is proved that DCR is an efficient and robust method in Brain Tumor Segmentation. Third, we conduct the decoder components and the low resolution feature map is expanded through the deconvolution operations, and then added with the feature extracted from DCR in upper layer. To the best of our knowledge, this work is the first to develop a deep learning framework using dilated convolution refine network for brain tumor segmentation. We evaluate our approach with Multimodal Brain Tumor Image Segmentation (BRATS 2015) dataset. The results show that our framework in complete tumor segmentation achieved excellent results with a DEC score of 0.87 and a PPV score of 0.92.

The rest of the paper is organized as following: the background of the dilated convolution technology and the brain tumor segmentation are introduced in section II, section III presents our framework, the experimental setup and results are shown and analyzed in section IV, and the paper is concluded by section V.

## II. RELATED WORK

During the image segmentation process, the larger receptive field of the network is conducive to the accurate detection and positioning of target objects. In order to obtain larger receptive fields, Chen *et al.* [5] and Yu *et al.*[6] have introduced dilated convolution, making the receptive field of the network is effectively increased without increasing the parameters of the convolution kernel. In addition, recent studies have shown that global vision is very useful in semantic segmentation [7-10]. Liang *et al.* [11] proposed the use of dilated convolution to extract dense features for semantic segmentation. In order to solve the multi-scale problem of segmented objects, the model is designed to use multi-proportional perforated convolution cascades or parallel to capture multi-scale receptive fields. PSPnet [12] takes many different sizes of images as input, it extracts highly abstract features through deeper layers network in small size images and details through shallow layers in large size images, the combination of these two features led to better segmentation results. In addition, the encoder-decoder framework is widely used in semantic segmentation. This framework mainly consists of two parts: (1) one part is the encoder process, in which a large field of receptivity is obtained through multiple downs-sampling and multiple layers of convolution overlap. (2) Another part is the decoder process, where the decoder recovers to the original image size through upsampling. For example, SegNet [13], Unet [14] and RefineNet [15] etc., use encoder-decoder framework achieved better semantic segmentation effects.

In recent years, research in the field of brain tumor segmentation has attracted the attention of researchers. Some traditional machine learning methods have been proposed. For example, Wu *et al.* [16] used the superpixel feature to segment brain tumors in the conditional random field framework, However there is a significant discrepancy results of the patients in different cases, especially has poor performance in LGG images. Pinto *et al.*[17] used random forests to segment features from tumor shape extraction, Soltaninejad *et al.*[18] combine extreme random tree classification with superpixel-based over segmentation for a single MRI scan. These methods above heavily rely on the specific experience knowledge of the appearance of the tumor, and the input dataset needs to have sufficiently high resolution features. However, collecting these features requires a lot of manual operations which results is inefficiency and low accuracy . In addition, there are also some non-machine learning models, for example, segmentation based on detection of specific shapes or connectivity detection etc. [19]. These non-machine learning models all share a common defect, i.e. relying heavily on human observation and subjective experience judgment.

Recently CNN is introduced to complete tumor segmentation. Zikic *et al.* [20] used a CNN model, consisting of two convolutional layers and a max-polling layer followed by a full connect (FC) layer and a softmax layer, to complete brain tumor segmentation. Havaei *et al.* [21] established a multi-pathway network structure, which combined local and global features in CNN, and used a local feature of a tumor image to classify a single pixel at a time. After multiple training, a complete segmentation result image was recovered. Sérgio [22] achieved the brain tumor segmentation It adopted a smaller $3\times3$ convolution kernel throughout the whole network, the model has good performance on the data BRATS2013. Hao *et al.* [23] used

Unet deep learning network structure to complete the tumor segmentation.

Although CNN has achieved great progress in brain tumor segmentation, it is still at the initial stage and need to be promoted. Based on the above discuss, we propose an automatic brain tumor segmentation network.

## III. APPROACH

### *A. the overview of the Brain Tumor Segmentation Network*

Usually, the network needs to obtain a receptive field as large as possible in the entire image during the semantic segmentation. But the brain tumor segmentation is quite different from the normal image semantic segmentation: (1) clinical medicine requires accurate segmentation, which can help for quantitative assessment of tumor geometry and guide to surgical planning. (2) the appearance and size of the tumor have strong variability and the process of extracting features of tumor is quite complexity Secondly; (3) there are differences in the image sampling protocols the inhomogeneity of the magnetic field and the partial volume effect will also have a great influence on the image quality obtained from conventionally 3D MRI images, thus affecting the accuracy of the algorithm.

Based on the above analysis, we come to know that the segmentation process requires that the model should not only consider receptive fields, but also pay more attention to the extraction of detailed features. A novel structure to overcome these deficiencies is proposed in Figure 2. As shown in Figure 2, based on the five blocks of the resnet-50 model, our proposed framework is divided into five slices. Slice i contains the input and output of this framework. The input is 224×224×4 MRI data. After the deconvolution operation on the right side, the prediction results with a dimension of 224×224×5 are obtained by a 1×1 convolution. In slice ii we design a DCR component, which will be explained in the next section, followed by the resnet-2. Because the feathers extracted by the resnet-2 are some detailed information, the idea of DCR we used here is to obtain the global view information of the tumor. In slice ii we set dilation-rate=12. and then, the features extracted from the DCR are fused with the feature map obtained from the Deconv-3, which come from slice iii. After this the fused feature maps are input into Deconv-4, which expand the 55×55×64 feature maps into 122×122×64 feature maps. The structure of slice iii is similar to slice ii. However due to the denser features compared to slice ii, we adjusted the dilated-rate of DCR to 6. Therefore slice iv and slice v have the similar structures, the only different is the dilated-rate which is in order to adapt the denser features. Specifically, the feature map obtained by resnet-5 of slice v is directly used as the input of Deconv-1,and does not merge with the feature map from the next layer.

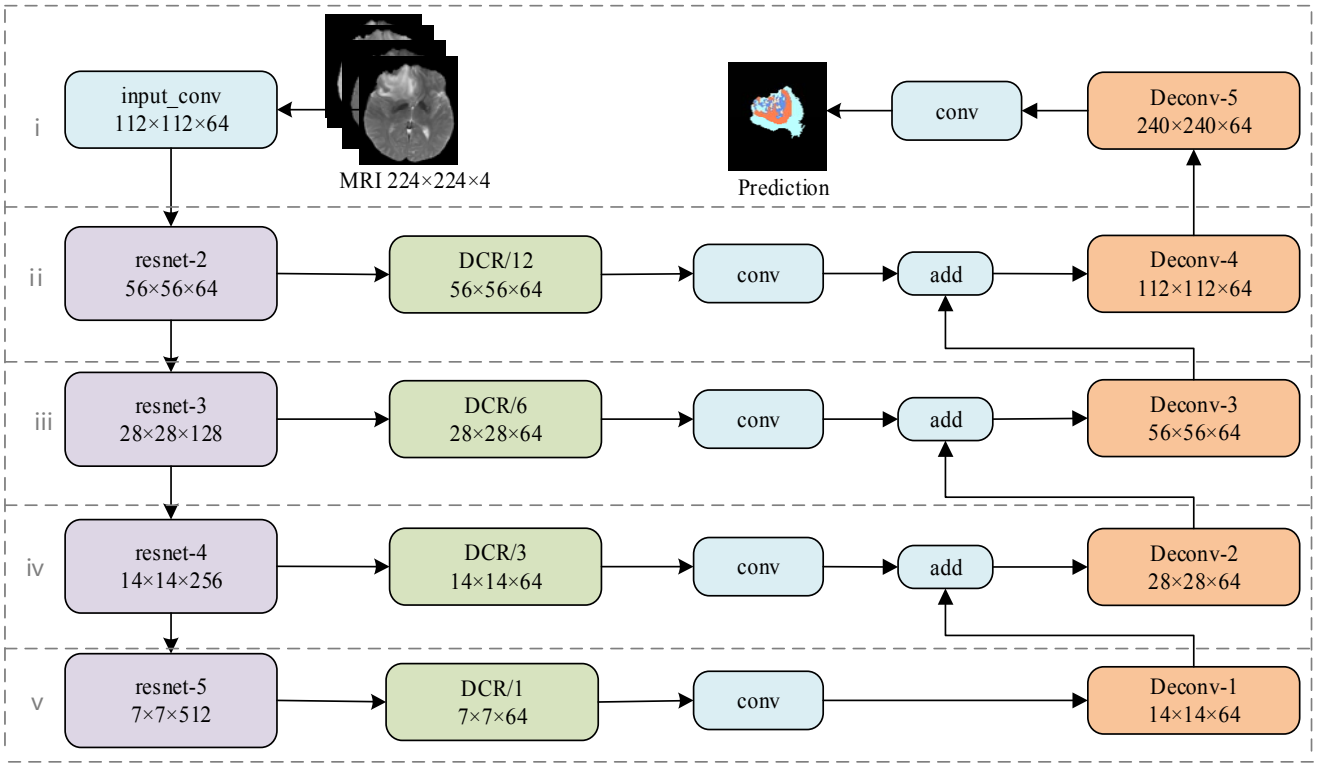


Fig. 2. The framework of Brain Tumor Segmentation pipeline

The purpose of this framework is to increase the sensitivity of the network to detailed information through the integrated use of multiple branches. In general, two aspects of innovation here are:

(1) Adopting a multi-path structure to complete the convolution process and improve the sensitivity of the network to details.

(2) Increase the receptive field of the network through different dilation rates.

### B. The function of DCR

On one hand, the receptive field of convolution kernel should be as large as possible from the perspective of semantic segmentation. This is conducive to setup comprehensive global view in the convolution kernel. On the other hand, from the perspective of information integrity, the high-level network of dilated convolution using sparse connection structure is easy to obtain original data information. Based on the above two principles, we propose a novel dilated convolution refine component (DCR) as shown in Figure 3. In this structure, it mainly consists of two parts. The first part is a 3×3 dilated convolution. The dilated rate in this component can be adjusted according to the actual situation to control the size of the receptive field in order to extract the global features. The second part adopts the residual structure. The 1×1point convolution can retain enough detail features. Through the combination of these two parts, the DCR component can effectively integrate rough global features and detail local features.

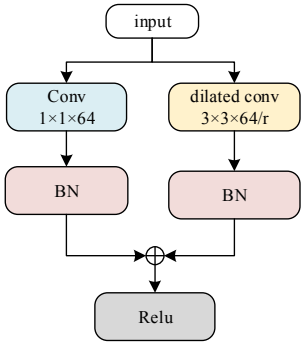

(A) DCR-A

Fig. 3. The structure of Dilated convolution refine(DCR)

### C. Decoder components

As showed on the left side of Figure 2, the output of the resnet-(n+1) is the half size of the resnet-n. If we want to add the feathers from lower layer to the upper layer, the feathers size need to be unified. Therefore， we design the decoder components. (i.e. Deconv-1, Deconv-2, …, and Deconv-5). For each Deconv component the low resolution feature map is expanded 2 times through the deconvolution operations, and then added with the feature extracted from DCR in upper layer. In the end the final output feature image of Deconv-1 has the same size as the input image of the framework, which is also the segmentation prediction result.

### D. Loss Function

Our training process includes two loss functions. The first one is the classification prediction loss, which calculates the cross-entropy between each pixel and the predicted value in the truth map:

$$\ell_{\alpha}^{i} = \alpha_{g}^{i} \bullet \log(\alpha_{p}^{i}) \tag{1}$$

The second is the content prediction loss, which calculates the pixel difference between the predicted value and the truth map. Because the absolute value difference between the two variables is not derivative, the loss function is calculated as below:

$$\ell_{\alpha}^{i} = \sqrt{(\alpha_{p}^{i} - \alpha_{g}^{i})^{2} + \varepsilon^{2}} \tag{2}$$

Where $\alpha_{p}^{i}$ represents the pixel value of the model prediction output layer at the i[th] pixel, $\alpha_{g}^{i}$ represents the pixel value of the i[th] pixel of the truth map， $\varepsilon$ is a constant, the value in the experiment is 10e-5. The reciprocal of this loss function is $\frac{\partial \ell_{\alpha}^{i}}{\partial \alpha_{p}^{i}}$ .

$$\frac{\partial \ell_{\alpha}^{i}}{\partial \alpha_{p}^{i}} = \frac{\alpha_{p}^{i} - \alpha_{g}^{i}}{\sqrt{(\alpha_{p}^{i} - \alpha_{g}^{i})^{2} + \varepsilon^{2}}} \tag{3}$$

In order to make the model more accurate prediction, the two loss functions are integrated in the training process, specifically as follows:

$$L = \mathrm{w}_{1} \bullet \sum_{i} \alpha_{g}^{i} \bullet \log(\alpha_{p}^{i}) + (1 - \mathrm{w}_{1}) \bullet \sum_{i} \sqrt{(\alpha_{p}^{i} - \alpha_{g}^{i})^{2} + \varepsilon^{2}} \tag{4}$$

Where $\mathrm{w}_{1}$ is a constant weight, and is set to 0.8 in this experiment. The loss function can calculate the pixel difference between the predicted image and the true-valued image, and the generated loss is calculated and transmitted back to each node in the network by the back-propagation method.

## IV. EXPERIMENT ESTABLISHMENT

We evaluate our approach using the standard benchmark BRATS2015 data set, which contains 220 HGG and 54 LGG patient MRI scan training data object samples. There are totally 110 test data object samples. Each sample in the data set is multi-modal MRI data, including sample data of Flair, T1, T1c, and T2. In our experiment a total of 42470

training images and 17050 test images are included. In the training process we use the standard Adam [24] optimization method and the batch size is 1, the initial learning rate is 1e-4, and all experiments are established based on the tensorflow1.4 [25] framework. We also initialize the parameters according to the Xavier [26] initialization method.

In order to increase the training data samples and improve the neural network model's robustness and generalization ability, in the experiments the input data is randomly fine-tuned through simple conversions such as flipping, rotating, shifting, and scaling, which can cause the image displacement to change, but does not result in training samples with large differences in shape.

### A. Evaluation indicators

In order to verify the validity of our model, the segmentation results are divided into three mutually exclusive tumor regions, which is more readable in clinical applications.

Specifically, the target segmentation tumor types in the experiment were divided into four types: necrosis, edema, and no enhancement and enhancement of tumors. The assessment phase combines them into 3 types, including:

*1) Complete:* Complete tumor area (all tumor type areas combined);

*2) Core:* The "core" area of the tumor (Including all tumor structures other than "edema");

*3) Enhancing:* "Enhance" of the tumor area (only contains the "enhanced core" structure unique to advanced cases).

Three commonly used scores were used for each tumor area to compare its segmentation effects (compare the gap between the generated mask and the truth map): Dice Similarity Coefficient (DSC), Positive Predictive Value (PPV) and Sensitivity (Sensitivity).

$$DSC=\frac{2TP}{FP+2TP+FN} \tag{5}$$

$$PPV=\frac{TP}{TP+FP} \tag{6}$$

$$Sensitivity=\frac{TP}{TP+FN} \tag{7}$$

In the above formula, the TP (True Positive) indicates the model predictions for true positive sample, TN (True Negative) indicates the prediction model for true negative sample, FP (False Positive) indicates the prediction model for false positive sample, and the FN (False Negative) indicates the model predictions for false negative sample. The DSC score, sensitivity and PPV are measures of the apparent overlap of voxels in the segmented regions. Different classes of scores assess different distances between segment boundaries (BRATS Experimental Center provides its online assessment system tool).

### B. Basic experiments

In order to evaluate the effectiveness of the DCR structure that proposed in Section III.B, we conduct two groups of controlled experiments, using BRATS 2015 as evaluation data. In addition to changing the dilated convolution refinement structure during the experiment, the rest of the parameters remain unchanged.

In the first group of experiments we explore the effectiveness of the DCR structure. As described in Section III.B, the DCR component can obtain the densely connection between feature maps. The main reason is that DCR uses a dilated convolution, the size of the convolution kernel is controlled by the dilation rate parameter. We use 1×1 convolution as the baseline. As shown in Figure 4(B), we first use a simple 1×1convolution to replace the DCR component. In Figure 4(C), a 3×3 dilated convolution is used also. In order to effectively compare the segmentation effects of these three structures, the remaining network structure and training parameters in DCR-A, DCR-B and DCR-C are remain unchanged. The results are presented in Table I.

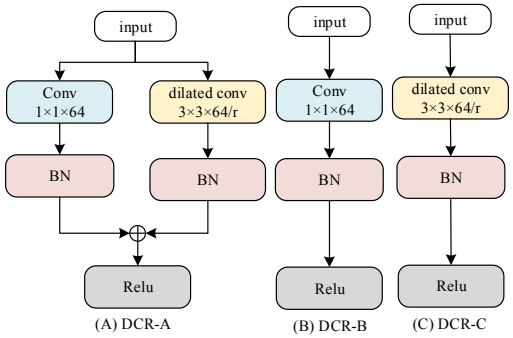


Fig. 4. (A) Dilated convolution refine network (B) 1×1 convolution baseline. (C) 3×3 dilated convolution.

TABLE I. EXPERIMENTAL RESULTS ON DIFFERENT DCR

| Method | DEC | | | PPV | | | Sensitivity | | |
|---|---|---|---|---|---|---|---|---|---|
| | *Complete* | *core* | *Enh.* | *Complete* | *core* | *Enh.* | *Complete* | *core* | *Enh.* |
| DCR-A | **0.87** | **0.62** | **0.68** | **0.92** | **0.65** | 0.86 | 0.8 | **0.62** | **0.59** |
| DCR-B | 0.85 | 0.57 | 0.60 | 0.89 | 0.59 | **0.89** | **0.83** | 0.57 | 0.47 |
| DCR-C | 0.84 | 0.55 | 0.59 | 0.90 | 0.58 | 0.87 | 0.80 | 0.56 | 0.48 |

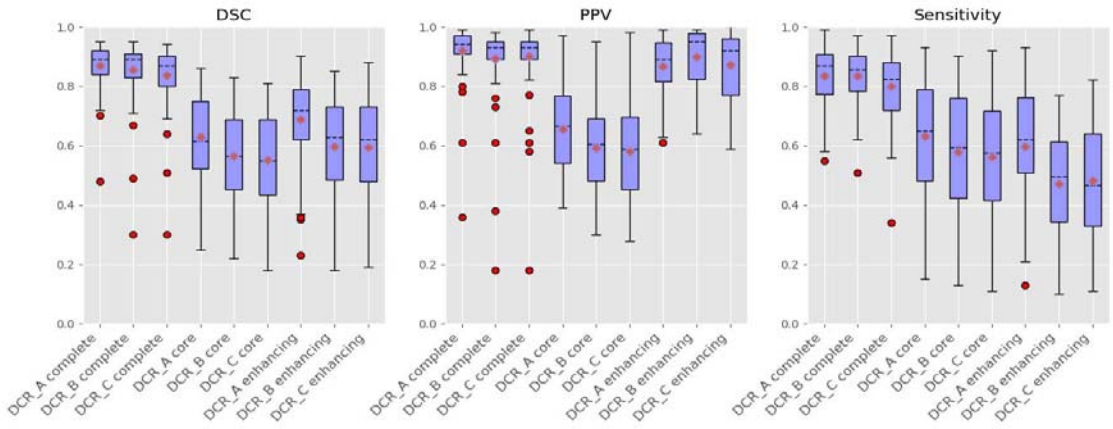


Fig. 5. Boxplot for each of the experiments in Table I in the BRATS2015.

Table I shows the DEC, PPV, and Sensitivity scores of DCR-A have significantly improved compared to the structure DCR-B with a 1×1 convolutional baseline and the structure DCR-C with a 3×3 dilated convolution. Specifically the DEC scores of enhancing tumor between DCR-A and DCR-B increased by 11.7%(i.e. (0.68-0.60)/0.68) and sensitivity increased by 18.6%(i.e. (0.59-0.48)/0.59). Comparing to DCR-C, the PPV scores of core tumor in DCR-A increase about 10.7% (i.e. (0.65-0.58)/0.65). We notice only under two set of parameters (i.e. the PPV score of enhancing tumor and the sensitivity scores of complete tumor in DCR-B), the DCR-B achieve better performance than DCR-A.

Figure 5 shows Boxplot for each of the experiments in Table I on the BRATS2015. The diamond marks the mean, the red dots indicate abnormal values. We observe a lower dispersion for the complete region within DSC, PPV and Sensitivity scores, which also presenting a higher mean value for the same region.

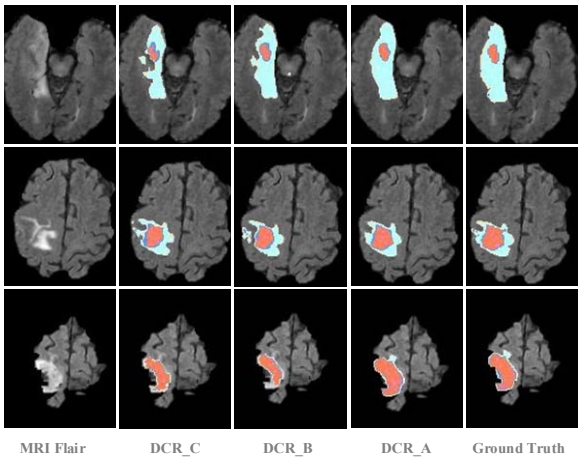


Fig. 6. Visual examples of semantic segmentation results in Table I.

Three visual comparisons are also given in Figure 6. It can be clearly seen that the DCR-A structural model results in a more complete and close to ground truth than the DCR-B structural and the DCR-C structural. In particular, the DCR-A structure model can maintain validity and guarantee the accuracy of segmentation edges.

In order to explore the influence of the dilation rate of the DCR dilated convolution on the network, we conduct the second group of experiments. We try different dilation rates, such as rate-1, rate-2 and rate-3. The parameters (12, 6, 3 and 1) represent the different dilation rate in different slice at Figure 2. As shown in Table II, our framework achieves the best results when the dilation rate is (12, 6, 3 and 1). In particular, the PPV scores of complete tumors, core tumors and enhancing tumors are increased by 2%, 1%, and 2%, respectively.

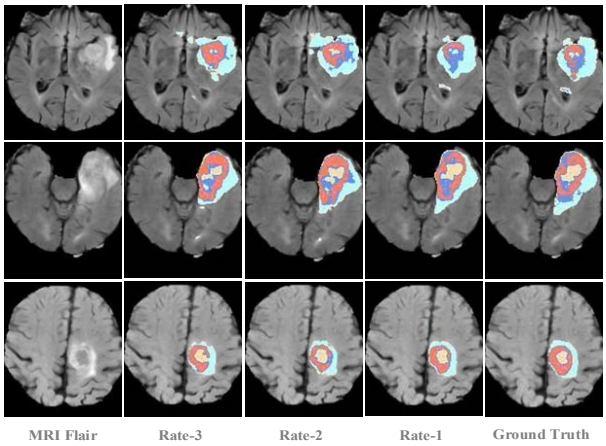


Fig. 7. Visual examples of semantic segmentation results in Table II.

Figure 7 shows the results of the three methods presented in Table II on the BRATS2015 online evaluation system. The diamond marks the mean, the red dots indicate the abnormal values. Three visual comparisons are given in Figure 8. It can be clearly seen that with the rate-1 parameter the DCR-A structural model performs better details information.

TABLE II. DCR-A EXPERIMENTAL RESULTS ON DIFFERENT DILATION RATES

| Dilated Rate | DEC | | | PPV | | | Sensitivity | | |
|---|---|---|---|---|---|---|---|---|---|
| | ***Complete*** | ***core*** | ***Enh.*** | ***Complete*** | ***core*** | ***Enh.*** | ***Complete*** | ***core*** | ***Enh.*** |
| Rate-1 (12,6,3,1) | **0.87** | 0.62 | 0.68 | **0.92** | **0.65** | 0.86 | 0.8 | 0.62 | 0.59 |
| Rate-2 (8,4,2,1) | 0.84 | **0.63** | 0.69 | 0.89 | 0.63 | 0.84 | **0.81** | 0.65 | 0.61 |
| Rate-3 (6,3,2,1) | 0.84 | 0.63 | **0.71** | 0.90 | 0.64 | 0.81 | 0.80 | **0.66** | **0.67** |

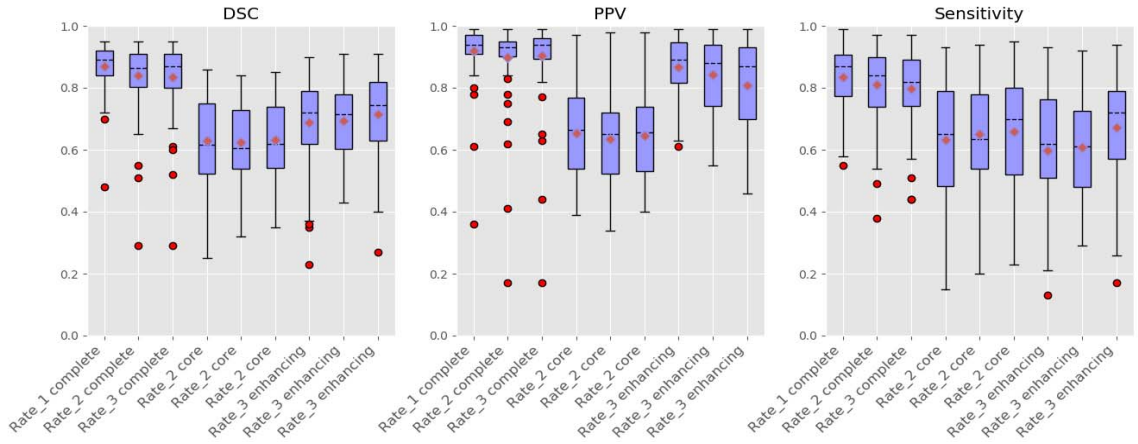


Fig. 8. Boxplot for different dilate rate of the experiments in Table II in the BRATS2015.

### C. *compare with state-of-the-arts segment methods*

In this subsection we discuss the specific performance of our model on the BRATS2015 dataset. Table 3 shows the results of the DSC，we compared the different deep learning models in the three papers recently published, from the table, we observe that our proposed model achieve the best DSC score in the complete tumor, which is about 0.87. In the core tumor and enhance tumor comparisons, our proposed model rank as third place.

After analyzing these results, we come to some reasons: (1) In the training data, the core and enhancing categories have insufficient sample size in the actual training process, and the network maybe overfitting; (2) The boundary between the enhanced tumor region and the non-enhancing tumor region is more diffuse and less obvious, and there are defects in the extraction of this fine-grained feature in the model. (3) In the general image segmentation, there are very few cases where instances contain instances. However, in the process of brain tumor segmentation, an instance often contains multiple instances.

TABLE III. EXPERIMENTAL RESULTS ON DIFFERENT METHODS

| **Method** | **DSC** | | |
|---|---|---|---|
| | ***Complete*** | ***core*** | ***Enh.*** |
| Havaei [21] | 0.79 | 0.58 | 0.69 |
| Kamnitsas[27] | 0.85 | **0.67** | 0.63 |
| Pereira[28] | 0.78 | 0.65 | **0.75** |
| **proposed** | **0.87** | 0.62 | 0.68 |

## V. CONCLUSION

An efficient and automatic image segmentation of brain tumor is still needed. In this paper, a novel automatic segmentation framework of brain tumors. We consider the impact of different structural parameters on the effectiveness of DCR, through two sets of comparative experiments, we explored the validity and rationality of DCR structure and parameters. The results of the BRATS 2015 online assessment system confirm that our best model has achieved good results in some evaluation indicators, we have successfully improved the latest methods currently released. Future work will focus on improving the robust reduce the computation time, In addition, we will evaluate proposed model in another BRATS datasets and longitudinal MRI images datasets.

ACKNOWLEDGMENTS: This work is supported by National Natural Science Foundation of China, under grant no. (61762089，61540061)

## REFERENCES

[1] N. R. Smoll, K. Schaller, and O. P. Gautschi, "Long-term survival of patients with glioblastoma multiforme (GBM)," *Journal of Clinical Neuroscience Official Journal of the Neurosurgical Society of Australasia,* vol. 20, no. 5, pp. 670-5, 2013.

[2] G. P. Mazzara, R. P. Velthuizen, J. L. Pearlman, H. M. Greenberg, and H. Wagner, "Brain tumor target volume determination for radiation treatment planning through automated MRI segmentation," *International journal of radiation oncology, biology, physics,* vol. 59, no. 1, p. 300, 2004.

[3] T. Yamahara *et al.*, "Morphological and flow cytometric analysis of cell infiltration in glioblastoma: a comparison of autopsy brain and neuroimaging," *Brain tumor pathology,* vol. 27, no. 2, pp. 81-87, 2010.

[4] B. Zhou, A. Khosla, A. Lapedriza, A. Oliva, and A. Torralba, "Object detectors emerge in deep scene cnns," *arXiv preprint arXiv:1412.6856,* 2014.

[5] L.-C. Chen, G. Papandreou, I. Kokkinos, K. Murphy, and A. L. Yuille, "Deeplab: Semantic image segmentation with deep convolutional nets, atrous convolution, and fully connected crfs," *arXiv preprint arXiv:1606.00915,* 2016.

[6] F. Yu and V. Koltun, "Multi-scale context aggregation by dilated convolutions," *arXiv preprint arXiv:1511.07122,* 2015.

[7] X. He, R. S. Zemel, and M. Á. Carreira-Perpiñán, "Multiscale conditional random fields for image labeling," in *Computer vision and pattern recognition, 2004. CVPR 2004. Proceedings of the 2004 IEEE computer society conference on*, 2004, vol. 2, pp. II-II: IEEE.

[8] J. Shotton, J. Winn, C. Rother, and A. Criminisi, "Textonboost for image understanding: Multi-class object recognition and segmentation by jointly modeling texture, layout, and context," *International Journal of Computer Vision,* vol. 81, no. 1, pp. 2-23, 2009.

[9] P. Kohli and P. H. Torr, "Robust higher order potentials for enforcing label consistency," *International Journal of Computer Vision,* vol. 82, no. 3, pp. 302-324, 2009.

[10] C. Russell, P. Kohli, and P. H. Torr, "Associative hierarchical crfs for object class image segmentation," in *Computer Vision, 2009 IEEE 12th International Conference on*, 2009, pp. 739-746: IEEE.

[11] L.-C. Chen, G. Papandreou, F. Schroff, and H. Adam, "Rethinking atrous convolution for semantic image segmentation," *arXiv preprint arXiv:1706.05587,* 2017.

[12] H. Zhao, J. Shi, X. Qi, X. Wang, and J. Jia, "Pyramid scene parsing network," in *IEEE Conf. on Computer Vision and Pattern Recognition (CVPR)*, 2017, pp. 2881-2890.

[13] V. Badrinarayanan, A. Kendall, and R. Cipolla, "Segnet: A deep convolutional encoder-decoder architecture for image segmentation," *IEEE transactions on pattern analysis and machine intelligence,* vol. 39, no. 12, pp. 2481-2495, 2017.

[14] O. Ronneberger, P. Fischer, and T. Brox, "U-net: Convolutional networks for biomedical image segmentation," in *International Conference on Medical image computing and computer-assisted intervention*, 2015, pp. 234-241: Springer.

[15] G. Lin, A. Milan, C. Shen, and I. Reid, "Refinenet: Multi-path refinement networks with identity mappings for high-resolution semantic segmentation," *arXiv preprint arXiv:1611.06612,* 2016.

[16] W. Wu, A. Y. C. Chen, L. Zhao, and J. J. Corso, "Brain tumor detection and segmentation in a CRF (conditional random fields) framework with pixel-pairwise affinity and superpixel-level features," *International Journal of Computer Assisted Radiology & Surgery,* vol. 9, no. 2, pp. 241-253, 2014.

[17] A. Pinto, S. Pereira, H. Correia, J. Oliveira, D. M. Rasteiro, and C. A. Silva, "Brain Tumour Segmentation based on Extremely Randomized Forest with high-level features," in *Engineering in Medicine and Biology Society*, 2015, p. 3037.

[18] M. Soltaninejad *et al.*, "Automated brain tumour detection and segmentation using superpixel-based extremely randomized trees in FLAIR MRI," *International Journal of Computer Assisted Radiology & Surgery,* vol. 12, no. 2, pp. 183-203, 2016.

[19] M. Prastawa, E. Bullitt, S. Ho, and G. Gerig, "A brain tumor segmentation framework based on outlier detection," *Medical image analysis,* vol. 8, no. 3, pp. 275-283, 2004.

[20] D. Zikic, Y. Ioannou, M. Brown, and A. Criminisi, "Segmentation of brain tumor tissues with convolutional neural networks," *Proceedings MICCAI-BRATS,* pp. 36-39, 2014.

[21] M. Havaei *et al.*, "Brain tumor segmentation with deep neural networks," *Medical image analysis,* vol. 35, pp. 18-31, 2017.

[22] S. Pereira, A. Pinto, V. Alves, and C. A. Silva, "Brain Tumor Segmentation Using Convolutional Neural Networks in MRI Images," *IEEE Transactions on Medical Imaging,* vol. 35, no. 5, p. 1240, 2016.

[23] H. Dong, G. Yang, F. Liu, Y. Mo, and Y. Guo, "Automatic Brain Tumor Detection and Segmentation Using U-Net Based Fully Convolutional Networks," in *Conference on Medical Image Understanding and Analysis*, 2017, pp. 506-517.

[24] D. P. Kingma and J. Ba, "Adam: A method for stochastic optimization," *arXiv preprint arXiv:1412.6980,* 2014.

[25] M. Abadi *et al.*, "Tensorflow: Large-scale machine learning on heterogeneous distributed systems," *arXiv preprint arXiv:1603.04467,* 2016.

[26] X. Glorot and Y. Bengio, "Understanding the difficulty of training deep feedforward neural networks," *Journal of Machine Learning Research,* vol. 9, pp. 249-256, 2010.

[27] K. Kamnitsas *et al.*, "Efficient multi-scale 3D CNN with fully connected CRF for accurate brain lesion segmentation," *Medical Image Analysis,* vol. 36, p. 61, 2016.

[28] S. Pereira, A. Pinto, V. Alves, and C. A. Silva, "Deep Convolutional Neural Networks for the Segmentation of Gliomas in Multi-sequence MRI," in *International Workshop on Brainlesion: Glioma, Multiple Sclerosis, Stroke and Traumatic Brain Injuries*, 2015, pp. 131-143.